Journal of Advanced Ceramics
2013, 2(3): 291–300
DOI: 10.1007/s40145-013-0075-8

ISSN 2226-4108
CN 10-1154/TQ

Research Article

Frequency and temperature dependent electrical characteristics of $CaTiO_3$ nano-ceramic prepared by high-energy ball milling

Subhanarayan SAHOO[a,*], Umasankar DASH[b], S. K. S. PARASHAR[c], S. M. ALI[a]

[a]*School of Electrical Engineering*, *KIIT University*, *Bhubaneswar 751024*, *India*
[b]*Center for Nanotechnology*, *KIIT University*, *Bhubaneswar 751024*, *India*
[c]*School of Applied Sciences*, *KIIT University*, *Bhubaneswar 751024*, *India*

Received: June 19, 2013; Revised: July 15, 2013; Accepted: July 21, 2013

Abstract: Nanocrystalline calcium titanate (CT) ceramic has been synthesized by a combination of solid-state reaction and high-energy ball milling. This nano-ceramic is characterized by X-ray diffraction (XRD), dielectric study and impedance spectroscopy. The XRD pattern shows single phase ceramic of orthorhombic symmetry. The frequency-dependent dielectric study shows that the dielectric constant is maximized at low frequencies and decreases with an increase in frequency. Impedance spectroscopy analyses reveal a non-Debye type relaxation phenomenon. A significant shift in impedance loss peaks toward the higher-frequency side indicates conduction in the material favoring the long-range motion of mobile charge carriers. The grain conduction effect is observed from the complex impedance spectrum by the appearance of one semicircular arc in Nyquist plot. It is also observed that the resistance decreases with an increase in temperature showing a negative temperature coefficient of resistance (NTCR). Various thermistor parameters have been calculated by fitting with Steinhart–Hart equation. The modulus plots represent the presence of temperature-dependent electrical relaxation phenomenon with the material. The frequency-dependent AC conductivity at different temperatures indicates that the conduction process is thermally activated. The activation energy has been calculated from an Arrhenius plot of DC conductivity and relaxation frequency.

Keywords: high-energy ball milling; dielectric study; impedance spectroscopy; thermistor; conductivity

1 Introduction

$CaTiO_3$ (CT) belongs to the important group of compounds with a perovskite-type structure which has been widely used in electronic devices, and it is a key component of synroc (a type of synthetic rock used to store nuclear waste) [1]. It has high dielectric constant, low dielectric loss and large temperature coefficient of resonant frequency, making it a promising component in the production of communication equipment operating at microwave frequencies (ultra high frequency (UHF) and super high frequency (SHF)), which in turn are used in microwave dielectric applications (as resonators and filters) [2–4]. Also, it is a material that can be employed as a thermally sensitive resistor element due to its negative temperature coefficient, and for the immobilization of highly radioactive wastes. Such unique properties give this material much attention, and many investigations regarding its many uses have been carried out in recent

* Corresponding author.
E-mail: subhanarayannanotech@gmail.com

years [5]. Recently, visible photoluminescence properties at room temperature in disordered structurally perovskite titanates ($CaTiO_3$) and highly emissive red-emitting phosphors have been reported in the literature [6–11] .

Different methods have been reported in the literature for the synthesis of $CaTiO_3$ powders. This perovskite was initially prepared by conventional solid-state reaction between TiO_2 and $CaCO_3$ or CaO at temperature of approximately 1623 K [12]. However, $CaTiO_3$ powders obtained by this method present several problems, such as high-processing temperature, inhomogeneity and contamination by impurities with a non-uniform particle size distribution [5]. To minimize these problems, wet chemical methods have been employed to synthesize $CaTiO_3$ powders with desired stoichiometry, such as sol–gel [2], co-precipitation [13], combustion method [14], organic–inorganic solution technique [15] and hydrothermal process [16].

High-energy ball milling has been used for many years in producing ultra fine powders of nano and submicron sizes. The severe and intense mechanical action on the solid surfaces leads to physical and chemical changes in the near surface region where the solids come into contact under mechanical forces. These mechanically initiated chemical and physicochemical effects in solids are generally termed as the mechanochemical effect. This route is currently being used to synthesize inorganic materials as it exhibits some advantages, such as the reduction in sintering temperature [17,18]. The study of the mechanochemical effect on fine particles has created much interest among researchers because of its several advantages to downstream processes like reducing annealing and sintering temperature, reducing phase transformation temperature, enhancing leaching process, decreasing thermal decomposition temperature, and increasing particle reactivity [19,20]. The mechanochemical synthesis process is carried out in high-intensity grinding mills such as vibro mills, planetary mills and oscillating mills. It has been noticed that the size reduction process and the microstructural evolution of $CaTiO_3$ during milling process are mainly influenced by the type of impulsive stress applied by the grinding media, which can either be an impact or shear type. Moreover, other parameters such as atmosphere composition and presence of different liquid media inside the grinding mill affect the mechanochemical process. In fact, when the mechanochemical synthesis of CaO and TiO_2 is carried out in planetary mills at higher rotational speeds to produce $CaTiO_3$, the impact stress is dominant, and not much attention is given on the mechanochemical mechanism itself.

The aim of this work, therefore, is to give an additional contribution in understanding the mechanochemical synthesis of $CaTiO_3$ nanoparticles without the deleterious phase and to study their electrical behavior via impedance and dielectric investigation.

2 Experiment

$CaTiO_3$ ceramic powders were prepared by high-energy ball milling technique. In this technique, CaO (99.9%) and TiO_2 (99.95%) were used as starting materials. Stoichiometric amounts of these materials were weighed. The high-energy ball milling of these weighed powders was done in Retsch High Energy ball mill. Initially, the weighed powders were mixed in tungsten carbide vial with tungsten carbide balls (10 mm in diameter) as milling media for 30 min at 100 rpm. The ball-to-powder ratio (BPR) was maintained at 20:1 by weight. Then it was increased to 300 rpm and high-energy milling was started. It was observed that the dry milling was not suitable for these materials because of sticking of powders to the walls of vials. To avoid this problem, toluene was added as a medium which also acted as a coolant and facilitated proper mixing of the powders during milling. Sampling was done every 5 h of milling. It was observed that CT phase was not formed even after 15 h of milling, the milled powders required further heat treatment to realize CT phase formation. To avoid the contamination, milling time was restricted to 15 h. After proper mixing, mixed powders were calcined at 600 ℃ for 2 h by an indigenous programmable furnace with intermediate grinding to avoid agglomeration of the particles. The calcined powders were used for the study of their phase formation as well as their reaction mechanism. After studying the phase formation, the powders were again ground and mixed with poly vinyl alcohol (PVA) (which acted as a binder) to reduce the brittleness, and have better compactness amongst the granules of the material. The green pellets with dimensions of 10 mm in diameter and 1 mm in thickness were made using a uniaxial press with the

help of tungsten carbide dye.

The synthesized powders were structurally characterized by X-ray diffraction (XRD) using a Philips diffractometer model PW-1830 with Cu Kα radiation ($\lambda = 1.5418$ Å) in a wide range of 2θ ($20° < 2\theta < 70°$) at a scanning rate of 2 (°)/min. In order to measure the electrical properties of CT ceramic, a disc was pressed uniaxially at 200 MPa with 2 wt% PVA added as a binder. Afterwards, this disc was sintered at 1200 ℃ for 2 h. Silver contacts were deposited on the opposite disc faces and heated at 700 ℃ for 15 min. The frequency (100 Hz–1 MHz) and temperature (300–500 ℃) dependent dielectric measurements were carried out using an LCR meter (HIOKI 3532 LCR HiTester) connected to a computer.

3 Results and discussion

3.1 XRD analysis

Figure 1 shows the XRD plots of $CaTiO_3$ powders ball-milled for different time durations at 300 rpm. It is observed that the powders ball-milled for 15 h show almost a single phase compound with a very small amount of impurity. The 15-h ball-milled powders were calcinied at 600 ℃ for 2 h. The XRD of the clacinied powders is shown in Fig. 2. The XRD figure shows a single phase material with orthorhombic structure in accordance with the ICDD No. 89-56. The average crystallite size is estimated by Scherrer's equation using the full width at half maximum (FWHM) of the most intense peak and found to be 90 nm. The lattice parameters are calculated to be $a = 5.3914(0)$ Å, $b = 5.4425(4)$ Å, and $c = 7.6526(4)$ Å.

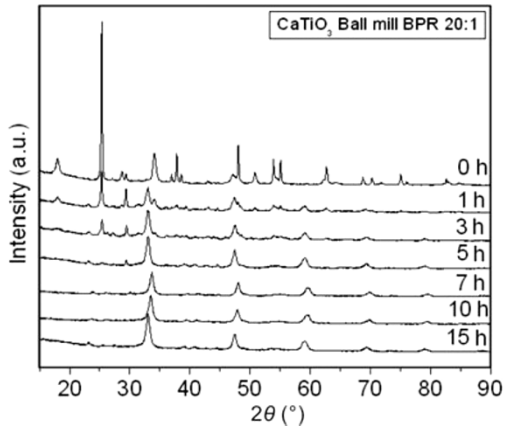

Fig. 1 XRD plots of $CaTiO_3$ powders ball-milled for different time durations.

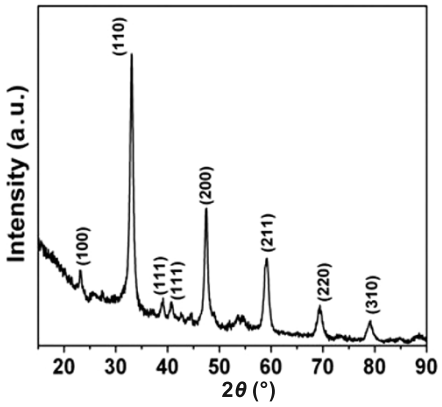

Fig. 2 XRD plot of $CaTiO_3$ powders ball-milled for 15 h and calcinied at 600 ℃ for 2 h.

3.2 Dielectric analysis

Figure 3(a) shows the variation of dielectric constant with respect to frequency at various temperatures. The nature of the dielectric permittivity for free dipoles oscillating in an alternating field may be described in the following way. At very low frequencies ($\omega \ll 1/\tau$, τ is the relaxation time), dipoles follow the field and we have $\varepsilon' = \varepsilon_s$ (value of the dielectric constant at quasistatic fields). As the frequency increases (with $\omega < 1/\tau$), dipoles begin to lag behind the field and ε' slightly decreases. When frequency reaches the characteristic frequency ($\omega = 1/\tau$), the dielectric constant drops (relaxation process). At very high frequencies ($\omega \gg 1/\tau$), dipoles can no longer follow the field and $\varepsilon' \approx \varepsilon_\infty$ (high-frequency value of ε'). Qualitatively this behavior has been observed in Fig. 3(a). The dielectric constant at low frequency is rather high, and is found to decrease with frequency at first and then becomes more or less stabilized. The high value of ε' at frequencies lower than 1 kHz, which increases with decreasing frequency and increasing temperature, corresponds to bulk effect of the system.

Figure 3(b) plots the angular frequency dependence of dielectric loss of $CaTiO_3$ at various temperatures. The dielectric loss is rather high at low frequency but falls quickly with rising frequency. Similar to the dependence of dielectric constant in temperature, the dielectric loss increases with increasing temperature. This indicates the thermally activated nature of the dielectric relaxation of the system. The fast rising trend of $\tan\delta$ at low frequencies is a representative of the presence of DC conductivity in CT ceramic. Higher values of dielectric constant interestingly observed

only at very high temperature and very low frequencies may be attributed to free charge buildup at the interfaces within the bulk of the sample (interfacial Maxwell–Wagner (MW) polarization [21]) and at the interface between the sample and the electrodes (space–charge polarization) [22].

3.3 Impedance spectroscopy study

Figure 4(a) shows the variation of the real part of impedance (Z') with frequency at various temperatures. It is observed that the magnitude of Z' decreases with increase in both frequency and temperature, indicating an increase in AC conductivity with rise in temperature and frequency. The Z' values for all temperatures merging at high frequency may be due to the release of space charges, as a result of reduction in barrier properties of the material with rise in temperature. Further, at low frequency Z' values decreases with increase in temperature show negative temperature coefficient of resistance (NTCR)-type behavior similar to that of semiconductors.

Figure 4(b) shows the variation of the imaginary part of impedance (Z'') with frequency at different temperatures. The curves show that Z'' values reach a maxima peak (Z''_{max}) and the value of Z''_{max} shifts to higher frequencies with increasing temperature. A typical peak broadening which is slightly asymmetrical in nature can be observed with the rise in temperature. The broadening of peaks in frequency explicit plots of Z'' suggests that there is a spread of relaxation time, i.e., the existence of a temperature-dependent electrical relaxation phenomenon in the material. The merger of Z'' values in the high frequency region may possibly be an indication of the accumulation of space charges in the material. The relaxation process may be due to the presence of immobile species at low temperature and defects at higher temperature.

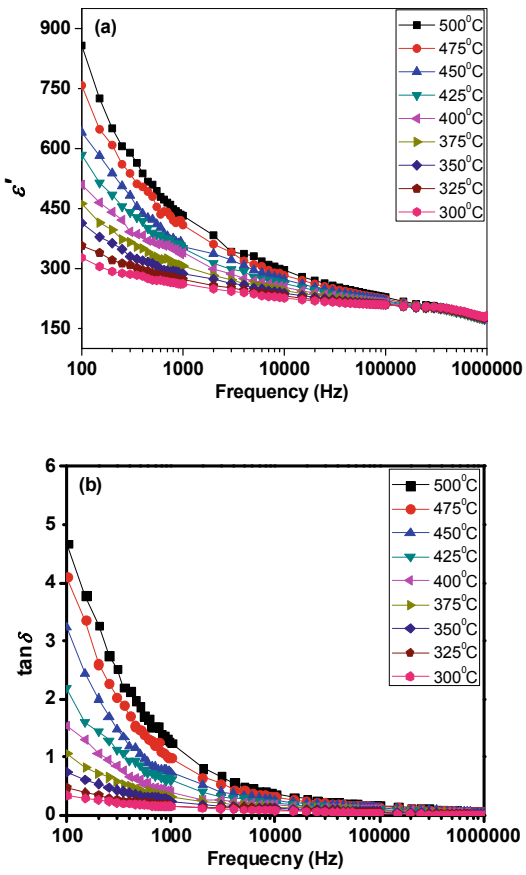

Fig. 3 Frequency-dependent (a) dielectric constant and (b) dielectric loss of $CaTiO_3$ at different temperatures.

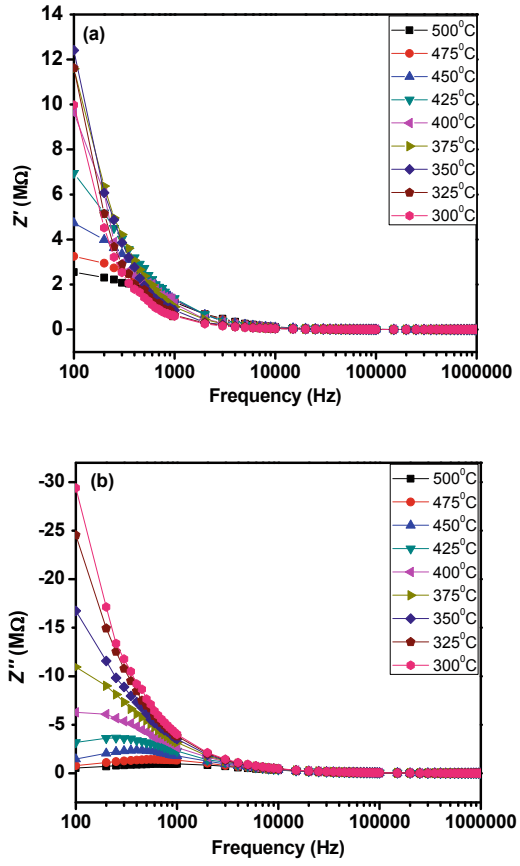

Fig. 4 Frequency-dependent variations of (a) real part Z' and (b) imaginary part Z'' for CT ceramic at different temperatures.

Figure 5 shows the complex impedance plots (Nyquist plots) of CT ceramic at different temperatures between 300 ℃ and 500 ℃. Single depressed semicircle is observed within the studied temperature range, representing the grain effect in the material. It is also observed that with the increase in temperature the radius of the semicircles decreases representing decrement in the resistivity. All the semicircles exhibit some depression degree instead of a semicircle centered at the real axis Z' due to a distribution of relaxation time. The bulk effect of the material is obtained by fitting the experimental response to that of an equivalent circuit, which is usually considered to comprise of one parallel resistor–CPE (constant phase element) elements. The circuit fitting parameter was done by ZView software with the modeled circuits. The experimental value of bulk resistance (R_b) at different temperatures has been obtained from the intercept of the semicircular arc on the real axis (Z'). The depression of the semicircle is considered further evidence of polarization phenomena with a distribution of relaxation time. This can be referred as the non-Debye type relaxation in which there is a distribution of relaxation time. This non-ideal behavior can be correlated to several factors, such as grain orientation, grain boundary, stress–strain phenomena and atomic defect distribution. This modification leads to Cole–Cole empirical behavior described by the following equation:

$$Z^* = R/(1+(\mathrm{j}\omega/\omega_0)^{1-n}) \quad (1)$$

where n represents the magnitude of the departure of the electrical response from an ideal condition and can be determined from the location of the center of the Cole–Cole circles. Least-squares fitting to the complex impedance data gives the value of $n>0$ at all the temperatures, suggesting the dielectric relaxation to be of poly-dispersive non-Debye type.

After performing the impedance spectroscopy data simulation, the calculated values of the equivalent electric circuit parameters were then related to the characteristic parameters. Results of the data simulation in a form of estimated parameters of the relaxation processes are given in Table 1.

Figure 6 shows both the experimental and simulated resistance values within the temperature range of 300–500 ℃. The simulated data has been obtained by performing Steinhart–Hart equation within the temperature range of 300–500 ℃.

From the graph we can conclude the experimental data are nearly equal to the simulated data. The experimental and simulated data both show NTCR property within the material, which signifies that nanocrystalline $CaTiO_3$ can be used as a promising environment-friendly material for high-temperature thermistor application. The Steinhart–Hart equation with the squared term eliminated is the most common

Table 1 Parameters obtained from temperature dependent impedance spectroscopy data for CT ceramic

Temperature (℃)	R (Ω)	C (F)
300	9.6525E7	8.2146E-12
325	7.2310E7	1.0928E-11
350	3.6844E7	2.1410E-11
375	2.5996E7	3.0043E-11
400	1.4624E7	5.3835E-11
425	9.0277E6	8.6176E-11
450	5.8032E6	6.7179E-11
475	3.7285E6	6.7649E-11
500	7.2358E6	7.2358E-11

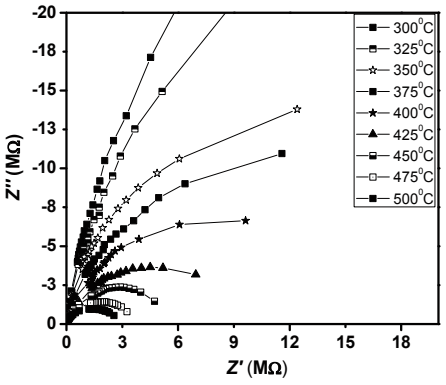

Fig. 5 Cole–Cole plots between Z' and Z'' for CT ceramic measured at various temperatures.

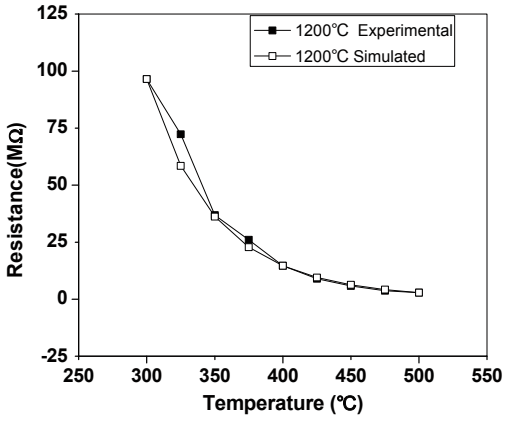

Fig. 6 Variations of both the experimental and simulated resistances.

form used and is usually found explicit in temperature T:

$$1/T = A + B\ln R + C(\ln R)^3 \quad (2)$$

where T is in kelvin unit; A, B and C are the curve fitting coefficients; and ln R is the natural logarithm of a resistance in ohm. Solving this equation set we obtain following values for fitting coefficients of Steinhart–Hart equation: $A = 0.000416221$, $B = 0.000034033$ and $C = 0.000000113$. Putting these results back into the above equation, we obtain the simulated value of resistances at corresponding temperatures. The A, B and C values obtained from the fitting are well within standard acceptable value of thermistor.

The β (known as sensitivity index of thermistor materials) value is a very important parameter in the description and specification of thermistor materials and thermistor components. The thermistor characteristic parameter can be expressed as

$$\beta = \left(\frac{TT_N}{T_N - T}\right)\ln\frac{R_T}{R_N} \quad (3)$$

where R_T is the resistance at temperature T; R_N is the resistance at temperature T_N known. Figure 7 shows β value in the temperature range of 300–500 ℃.

α is a material characteristic which shows the resistance change percentage per degree centigrade. The temperature coefficient is a basic concept in thermistor calculation.

$$\alpha = (1/R)[\mathrm{d}(R)/\mathrm{d}T] = -\beta/T^2 \quad (4)$$

Because the resistance of NTCR thermistor is a function of temperature, the α value of a particular thermistor material is also nonlinear across the relevant temperature range. The variation of α parameter with temperature is shown in Fig. 8. For the usual thermistor materials β constant is closely related to

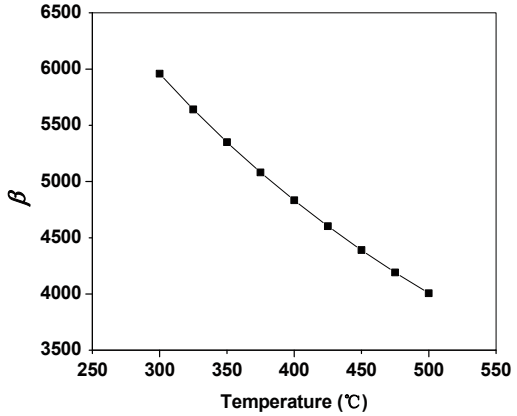

Fig. 7 Variation of β value with temperature.

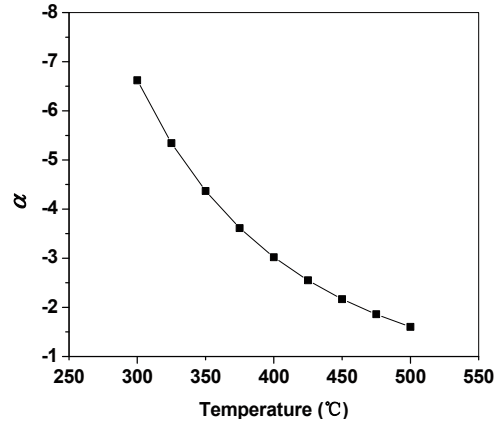

Fig. 8 Variation of α value with temperature.

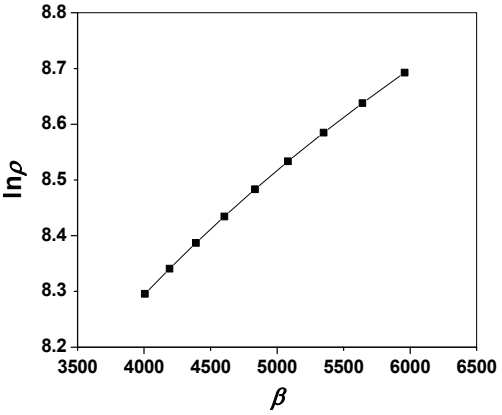

Fig. 9 Variation of $\ln\rho$ with β.

resistivity as shown in Fig. 9. The general information on sensitivity of material resistivity to temperature can be interpreted from the β value indicated in Fig. 9. It is well known that material having high β value has high temperature stability. Here we got β value in the range of 4000–6000 K, which means CT ceramic is capable to withstand temperature surges and very suitable in high temperature electronic applications.

3.4 Electrical modulus

In order to clarify whether the multiple relaxations and/or conduction processes are involved in the complex dielectric response of $CaTiO_3$, ceramics are given with the dielectric modulus formalism in addition to the complex permittivity analysis. The complex dielectric modulus corresponds to the relaxation of the electric field in the material when the electrical induction D is maintained as constant and defined as

$$M^*(f) = \frac{1}{\varepsilon^*} = M'(f) + \mathrm{i}M''(f) \quad (5)$$

The frequency dependence of the imaginary part of the

dielectric modulus $M''(f)$ at various temperatures generally provides information concerning the charge transport mechanism such as electrical transport and conductivity relaxation, and has been successfully used to distinguish localized dielectric relaxation processes from long-range conductivity and short/long-range polaron hoping in ceramics. A conductivity relaxation is indicated by the presence of a peak in the imaginary part of the dielectric modulus spectrum not accompanied by a peak in the imaginary part of the permittivity, while a dielectric relaxation phenomenon gives maxima both in the imaginary parts of permittivity and of dielectric modulus spectra.

Figures 10(a) and 10(b) display the (angular) frequency dependence of $M'(\omega)$ and $M''(\omega)$ for CT ceramic at different temperatures. $M'(\omega)$ shows a dispersion tendency toward M_∞ (the asymptotic value of $M'(\omega)$ at higher frequencies. In the low-temperature region, the value of $M'(\omega)$ increases with the increase in frequency and decreases with rise in temperature with slow rate, while in the high-temperature region, the value of $M'(\omega)$ increases rapidly with the increase in both temperature and frequency. It may be contributing to the conduction phenomena due to the short range mobility of charge carriers. This implies the lack of a restoring force for flow of charges under the influence of a steady electric field.

Figure 10(b) shows the frequency dependence of the imaginary part $M''(\omega)$ of the electric modulus at different temperatures. The plots show an asymmetric behavior with respect to peak maxima whose positions are frequency and temperature dependent. These spectra also reflect the motions of the ions in the material by exhibiting two apparent relaxation regions. The left region of the peak indicates the conduction process, while region on the right of the peak is associated to the relaxation process where the ions can make localized motion within the well. The asymmetric modulus peak shifts towards higher-frequency side exhibiting the correlation between the motions of mobile charge carriers. The asymmetry in peak broadening shows the spread of relaxation time with different time constant, and hence the relaxations of non-Debye type. The existence of low-frequency peaks suggests that the ions can move over long distances, whereas high-frequency peaks suggest about

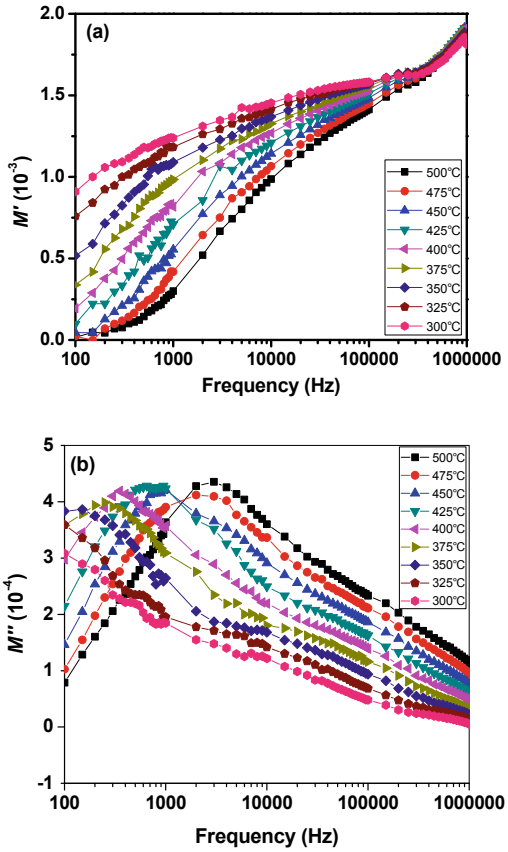

Fig. 10 Frequency dependent variations of (a) real part $M'(\omega)$ and (b) imaginary part $M''(\omega)$ for the CT ceramic with at different temperatures.

the confinement of ions in their potential well. The nature of modulus spectrums confirms the existence of hopping mechanism in the electrical conduction of the materials.

The frequency ω_m (corresponding to Z''_{max} and M''_{max}) gives the most probable relaxation time τ_m from the condition $\omega_m\tau_m = 1$ .The most probable relaxation time follows the Arrhenius law, given by

$$\omega_m = \omega_0 \exp\left(\frac{-E_a}{k_B T}\right) \tag{6}$$

where ω_0 is the pre-exponential factor; k_B is Boltzman constant; and E_a is the activation energy. Figure 11 shows a plot of $\log\omega_m$ versus $1/T$, where the dots are the experimental data and the solid lines are the least-squares straight-line fit from the relaxation of both Z'' and M''. The activation energy E_a were calculated from the least-squares fit to the points. From Fig. 11 it can be seen that the activation energy calculated from Arrhenius relation

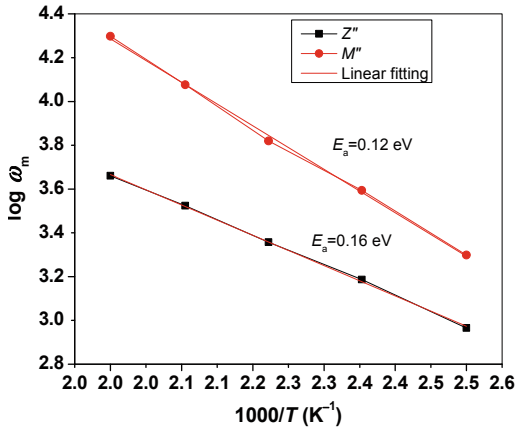

Fig. 11 Arrhenius plots of $\log\omega_m$ from imaginary part of (a) impedance and (b) modulus.

are $E_a = 0.16$ eV for Z'' and $E_a = 0.12$ eV for M''.

3.5 Conductivity

The AC electrical conductivity was obtained in accordance with the relation $\sigma_{AC} = d/(A \cdot Z')$, where d is the thickness and A is the surface area of the specimen. Figure 12 shows the variation of AC electrical conductivity σ_{AC} of CT ceramic as a function of frequency at different temperatures. The conductivity plot possesses the following characteristics: (i) dispersion at lower and merging at higher frequencies of conductivity spectra with the increase in temperature. The plot shows conductivity increases with increase of temperature. Frequency independent behavior of the conductivity in the low-frequency region is observed but that becomes sensitive at high-frequency region, which is generally known as hopping frequency, shifted towards higher-frequency side with increase of temperature. In the higher-frequency region, the conductivity increases due to the hopping of charge carriers in finite clusters. Frequency independent AC conductivity observed in the high temperature indicates the long-range movement of mobile charge carriers. The high frequency variation of σ_{AC} is found to obey universal Jonscher's power law behavior, $\sigma_{AC} = K\omega^s$, with $0 \leqslant s \leqslant 1$, where ω is the angular frequency of AC field, in the frequency sensitive region.

Figure 13 shows the variation of σ_{DC} against the $10^3/T$. The value of bulk conductivity of the material is evaluated from the AC conductivity plot of the sample at different temperatures by theoretical fitting using Joncher's power law. At higher temperature, the conductivity versus temperature response is more or less a straight line and can be explained by a thermally activated transport of Arrhenius type:

$$\sigma_{DC} = \sigma_0 \exp\left(\frac{-E_a}{k_B T}\right) \tag{7}$$

where σ_0, E_a and k_B represent the pre-exponential term, the activation energy of the mobile charge carriers and Boltzmann's constant, respectively. At lower temperature, a small deviation from the linear behavior of conductivity has been noticed and can be attributed to Mott's hopping type phenomena. The DC activation energy of the material has been estimated to 0.12 eV in the temperature. The activation energy values for the electric modulus (0.11 eV) and for DC conductivity (0.11 eV) are almost identical suggesting a hopping mechanism for CT ceramic.

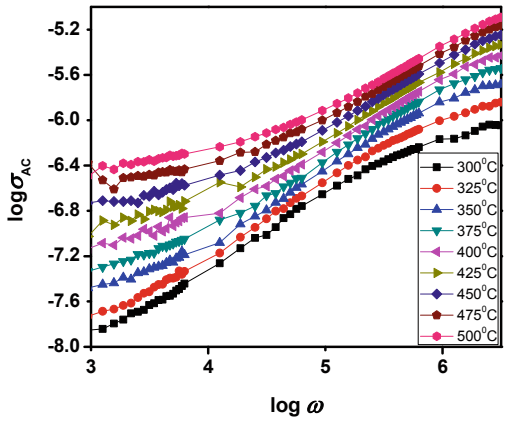

Fig. 12 Frequency dependence of AC conductivity of CT ceramic at different temperatures.

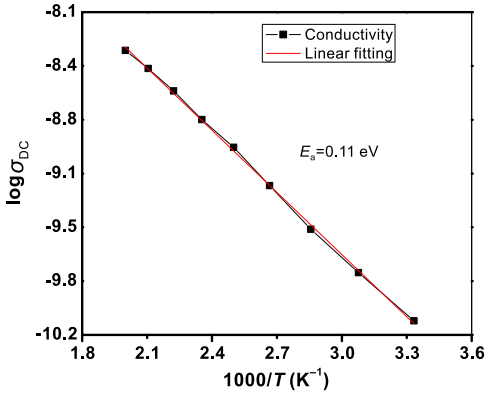

Fig. 13 Temperature dependence of DC conductivity for CT ceramic. The dots are the experimental points and the solid lines are the least-squares straight line fit.

4 Conclusions

Nanocrystalline calcium titanate ceramic has been prepared by a high-energy ball milling technique. X-ray analysis confirms the orthorhombic structure. The temperature-dependent dielectric study reveals a normal ferroelectric behavior in the material. Electrical parameters such as the real part of impedance (Z'), the imaginary part of impedance (Z'') and AC/DC conductivity as functions of both frequency and temperature have been studied through impedance spectroscopy. Nyquists plots show bulk effect and the resistance decreases with rise in temperature, which indicates the NTCR behavior of the sample. The thermistor parameter has been obtained by the standard equations. It is found that the values of the parameters obtained from the experimental results are in accordance with the other thermistor used in industries. The electrical relaxation process occurring in the material has been found to be temperature dependent. Modulus analysis has established the possibility of hopping mechanism for electrical transport processes in the system. The AC conductivity spectrum is found to obey Jonscher's universal power law. The frequency-dependent AC conductivity at different temperatures indicates that the conduction process is thermally activated. In particular, a high-performance NTCR thermistor is important because the thermistor should detect temperature over a wide range and under very severe condition. The thermistor obeying Steinhart–Hart equation means all the prepared sample useful for high temperature applications with rapid thermal response.

References

[1] Lutze W, Ewing RC, Eds. *Radioactive Waste Forms for the Future*. Amsterdam: Elsevier, 1988: 233–334.

[2] Pfaff G. Synthesis of calcium titanate powders by the sol–gel process. *Chem Mater* 1994, **6**: 58–62.

[3] Cavalcante LS, Marques VS, Sczancoski JC, *et al*. Synthesis, structural refinement and optical behavior of $CaTiO_3$ powders: A comparative study of processing in different furnaces. *Chem Eng J* 2008, **143**: 299–307.

[4] Cavalcante LS, Simões AZ, Santos LPS, *et al*. Dielectric properties of $Ca(Zr_{0.05}Ti_{0.95})O_3$ thin films prepared by chemical solution deposition. *J Solid State Chem* 2006, **179**: 3739–3743.

[5] Evans IR, Howard JAK, Sreckovic T, *et al*. Variable temperature in situ X-ray diffraction study of mechanically activated synthesis of calcium titanate, $CaTiO_3$. *Mater Res Bull* 2003, **38**: 1203–1213.

[6] Marques VS, Cavalcante LS, Sczancoski JC, *et al*. Synthesis of $(Ca,Nd)TiO_3$ powders by complex polymerization, Rietveld refinement and optical properties. *Spectrochim Acta A* 2009, **74**: 1050–1059.

[7] de Lazaro S, Milanez J, de Figueiredo AT, *et al*. Relation between photoluminescence emission and local order–disorder in the $CaTiO_3$ lattice modifier. *Appl Phys Lett* 2007, **90**: 111904.

[8] Pan Y, Su Q, Xu H, *et al*. Synthesis and red luminescence of Pr^{3+}-doped $CaTiO_3$ nanophosphor from polymer precursor. *J Solid State Chem* 2003, **174**: 69–73.

[9] Haranath D, Khan AF, Chander H. Bright red luminescence and energy transfer of Pr^{3+}-doped $(Ca,Zn)TiO_3$ phosphor for long decay applications. *J Phys D*: *Appl Phys* 2006, **39**: 4956.

[10] Zhang X, Zhang J, Nie Z, *et al*. Enhanced red phosphorescence in nanosized $CaTiO_3:Pr^{3+}$ phosphors. *Appl Phys Lett* 2007, **90**: 151911

[11] Okamoto S, Kobayashi H, Yamamoto H. Enhancement of characteristic red emission from $SrTiO_3:Pr^{3+}$ by Al addition. *J Appl Phys* 1999, **86**: 5594.

[12] Kay HF, Bailey PC. Structure and properties of $CaTiO_3$. *Acta Cryst* 1957, **10**: 219–226.

[13] Zhang X, Zhang J, Ren X, *et al*. The dependence of persistent phosphorescence on annealing temperatures in $CaTiO_3:Pr^{3+}$ nanoparticles prepared by a coprecipitation technique. *J Solid State Chem* 2008, **181**: 393–398.

[14] Muthuraman M, Patil KC, Senbagaraman S, *et al*. Sintering, microstructural and dilatometric studies of combustion synthesized synroc phases. *Mater Res Bull* 1996, **31**: 1375–1381.

[15] Lee SJ, Kim YC, Hwang JH. An organic–inorganic solution technique for fabrication of nano-sized $CaTiO_3$ powder. *J Ceram Process Res* 2004, **5**: 223–226.

[16] Kutty TRN, Vivekanandan R, Murugaraj P. Precipitation of rutile and anatase (TiO_2) fine powders and their conversion to $MTiO_3$ (M = Ba, Sr, Ca) by the hydrothermal method. *Mater Chem Phys*

1988, **19**: 533–546.

[17] Kong LB, Zhu W, Tan OK. Preparation and characterization of $Pb(Zr_{0.52}Ti_{0.48})O_3$ ceramics from high-energy ball milling powders. *Mater Lett* 2000, **42**: 232–236.

[18] German RM. *Sintering Theory and Practice*. New York: Wiley, 1996.

[19] Wang J, Xue JM, Wan DM, *et al*. Mechanically activating nucleation and growth of complex perovskites. *J Solid State Chem* 2000, **154**: 321–328.

[20] Siqueira JRR, Simões AZ, Stojanovic BD, *et al*. Influence of milling time on mechanically assisted synthesis of $Pb_{0.91}Ca_{0.1}TiO_3$ powders. *Ceram Int* 2007, **33**: 937–941.

[21] Bidault O, Goux P, Kchikech M, *et al*. Space charge relaxation in perovskites. *Phys Rev B* 1994, **49**: 7868–7873.

[22] Kyritsis A, Pissis P, Grammatikakis J. Dielectric relaxation spectroscopy in poly(hydroxyethy acrylate)/water hydrogels. *J Polym Sci Pol Phys* 1995, **33**: 1737–1750.